Next Materials 9 (2025) 101313

Contents lists available at ScienceDirect

Next Materials

journal homepage: www.sciencedirect.com/journal/next-materials

Research article

# Effect of variation in hydrogen content on catalytic properties of $Zr_7Ni_{10}$ hydrogen storage alloy

Shu Mizutome [a,b], Nodoka Sasaki [a], Kohta Asano [c], Kouji Sakaki [c], Ya Xu [d], Satoshi Kameoka [b,*]

[a] Department of Materials Processing, Graduate School of Engineering, Tohoku University, Japan
[b] Institute of Multidisciplinary Research for Advanced Materials, Tohoku University (IMRAM), Japan
[c] Energy Process Research Institute, National Institute of Advanced Industrial Science and Technology (AIST), Japan
[d] Research Center for Energy and Environmental Materials, National Institute for Materials Science (NIMS), Japan

ARTICLE INFO

*Keywords:*
Hydrogen storage alloy catalyst
$Zr_7Ni_{10}$
Hydrogenation of acetylene
Hydrogen content
Absorbed hydrogen

ABSTRACT

Hydrogen storage alloys are expected to be catalyst materials for the hydrogenation of hydrocarbons and carbon dioxide. The role of hydrogen absorbed in the hydrogen storage alloy catalysts has been investigated from the perspectives of the hydrogen supplying itself as a reactive species and changing the chemical state of the alloy catalysts. However, few studies have considered the catalysts' hydrogen storage properties under the reaction fields. To investigate the relationship between the hydrogen storage properties and the catalytic properties, we focus on $Zr_7Ni_{10}$ alloy, which exhibits a unique phase-transition process involving two hydride phases (β phase and γ phase) and a broad solid-solution region of the hydrogen solid-solution phase (α phase). The catalytic properties of $Zr_7Ni_{10}$ were examined for the hydrogenation of acetylene under conditions where the phase transitions occurred and the hydrogen content of the α phase varied. The results showed that the α phase exhibited higher rates of acetylene conversion than the degassed alloy. Below 230 °C, where the phase transitions occurred, $Zr_7Ni_{10}$ showed higher catalytic activity with increasing temperature but the difference among the phases could not be observed. However, above 230 °C, where the hydrogen content of the α phase decreased with increasing temperature, the catalytic activity also decreased. During the subsequent cooling process, where the hydrogen content of the α phase increased, the catalytic activity recovered. Considering a board solid-solution region of the α phase, we concluded that the variation in hydrogen content of the α phase induced the reversible catalytic activity behavior.

## 1. Introduction

Hydrogen storage alloys, which store hydrogen in a metal lattice by forming the hydride phase, are expected to be catalyst materials for the hydrogenation of hydrocarbons and carbon dioxide [1–10]. In particular, they have been attracting attention as catalysts for hydrogenation, in which hydrogen atoms are added to unsaturated carbon–carbon and carbon–oxygen bonds. The effect of absorbed hydrogen on the hydrogenation reactions has been discussed from two main perspectives. The first perspective involves the supply of atomic hydrogen with high reactivity. When absorbed hydrogen is desorbed into the gas phase, it can be considered to be in the atomic state on the alloy surface, thus, absorbed hydrogen may be a reactive species in the hydrogenation reactions. Soga *et al.* have reported this possibility for $LaNi_5$ as a catalyst in the hydrogenation of ethylene [11]. They revealed that 90 % of the hydrogen that reacted with ethylene came from absorbed hydrogen. This result indicates that absorbed hydrogen is more reactive than hydrogen adsorbed from the gas phase onto the alloy surface. Kato *et al.* have reported the same possibility for ZrCo as a methanation catalyst [12]. These previous studies have demonstrated that hydrogen storage alloys can provide a novel transport pathway for hydrogen, delivering it from the bulk interior to the reactants on the alloy surface.

The second perspective from which hydrogen storage alloys are promising as catalyst materials is that absorbed hydrogen can alter the electronic state of the alloys, consequently affecting the reactivity of reactants on the alloy surface [13]. Tsukuda *et al.* have reported this effect for $ErNi_{3.75}Al_{1.25}$ and $Mg_2Ni$ in the hydrogenation of ethylene [14]. They found that the hydride phase of $ErNi_{3.75}Al_{1.25}$ exhibited a

* Corresponding author.
*E-mail address:* satoshi.kameoka.b4@tohoku.ac.jp (S. Kameoka).

https://doi.org/10.1016/j.nxmate.2025.101313
Received 22 July 2025; Received in revised form 29 September 2025; Accepted 6 October 2025

lower adsorption capacity and higher catalytic activity than the alloy phase. By contrast, $Mg_2Ni$ showed the inverse trend, where the hydride phase exhibited a higher adsorption capacity and lower catalytic activity than the alloy phase. These results for $ErNi_{3.75}Al_{1.25}$ and $Mg_2Ni$ suggested that absorbed hydrogen does not always enhance the catalytic activity. The ability of absorbed hydrogen to change the adsorption capacity and, consequently, the catalytic activity is an active discussion topic in terms of electronic state. Tsukuda *et al*. mentioned that absorbed hydrogen supplies an electron to a Ni-*d* antibonding orbital in $ErNi_{3.75}Al_{1.25}$ and decreases the adsorption capacity of the reactant, and it is also noted that Pd shows a similar trend [15]. Recently, this mechanism was applied to improve the selectivity in hydrogenation of acetylene by providing a favor environment for the adsorption of acetylene and the desorption of ethylene [16,17]. Thus, the effects of absorbed hydrogen on the electronic structure and catalytic properties have attracted considerable attention.

To investigate the effect of absorbed hydrogen on the catalytic properties of alloys, previous related studies have compared the catalytic properties of hydrogen-absorbed and hydrogen-desorbed catalysts. By contrast, few studies have investigated the effect of the variation of the hydrogen content on the catalytic properties. To address this knowledge gap, we here investigate the catalytic properties of $Zr_7Ni_{10}$ alloy, whose hydrogen storage properties differ from those of general alloys from two perspectives. The first perspective is the difference in the phase-transition processes between hydrogenation and dehydrogenation for the $Zr_7Ni_{10}$–$H_2$ system. In the hydrogenation process, $Zr_7Ni_{10}$ transforms from the hydrogen solid-solution phase (α phase) to the full hydride phase (γ phase), whereas, in the dehydrogenation process, it undergoes two phase transitions via the intermediate hydride phase (β phase) [18–24]. This difference in phase transitions between hydrogenation and dehydrogenation might affect the catalytic properties. The second perspective is the fluctuating hydrogen content of the α phase [21]. This property is evident from the difference in the hydrogen content when the α phase appears during the hydrogenation and dehydrogenation. Additionally, $Zr_7Ni_{10}$ has a broad solid-solution region up to approximately 0.5H/M, indicating a continuous variation in the hydrogen content. Therefore, examining the catalytic properties of the α phase allows for a clear comparison under various hydrogen contents within the same phase. If absorbed hydrogen is involved in catalytic processes, the phase transitions and the variation in the hydrogen content of the $Zr_7Ni_{10}$ alloy should also be reflected in its catalytic properties. In the present study, $Zr_7Ni_{10}$ hydrogen storage alloy is used as a catalyst for the hydrogenation of acetylene and the relationship between its hydrogen storage properties and catalytic properties is investigated.

## 2. Experimental

### 2.1. Material preparation

$Zr_7Ni_{10}$ was synthesized by arc melting. The raw materials were Zr (99.6 %) and Ni (99 +%). A Ti getter was melted in advance to purify the Ar atmosphere in the arc melting furnace. Arc melting was conducted five times, and the ingot was turned over after each process. To improve the homogeneity of the alloy, it was annealed for 48 h at 1173 K under Ar and cooled in a furnace. The obtained alloy sample was pulverized and sieved to achieve a particle size distribution between 25 and 63 μm. The crystal structure of the sample was determined by powder X-ray diffraction (XRD; Rigaku Ultima IV) using Cu-Kα radiation. The crystal structure was analyzed by the Rietveld method using the EXPO2014 software [25]; space group *Cmce* was used for the crystal symmetry (notably, the space group was previously described as *Cmca*, but *Cmce* and *Cmca* are crystallographically equivalent) [26–30].

### 2.2. Hydrogen storage properties

The hydrogenation and dehydrogenation properties for the $Zr_7Ni_{10}$–$H_2$ system were investigated by pressure-composition-isotherms (PCIs) acquired using the Sieverts method. Approximately 2 g of the powder sample was transferred to a stainless-steel reactor. After several cycles of hydrogen gas being introduced into and then evacuated from the reactor at room temperature, hydrogen gas was introduced into the reactor to 3 MPa and the sample was then heated to 150 °C. The hydrogen gas in the reactor was subsequently evacuated, and the sample was additionally heated at 300 °C for 1 h under vacuum. After these pretreatments, the PCIs were measured at 150, 200, and 300 °C.

The phase transition process for the $Zr_7Ni_{10}$–$H_2$ system was investigated by differential scanning calorimetry (DSC) under a $H_2$ atmosphere using a differential scanning calorimeter (Rigaku DSC8230HP). The $H_2$ pressure was set to 0.1 MPa to match the catalytic test conditions described later. To obtain the full hydride phase of the γ phase, approximately 10 mg of the sample was heated to 350 °C at a heating rate of 5 °C/min under 0.1 MPa-$H_2$ and then cooled to room temperature at a cooling rate of 5 °C/min. After this pretreatment, DSC curves were obtained at heating and cooling rate of 2, 5 and 10 °C/min. The phase-transition temperatures were determined from the exothermic and endothermic peaks in the DSC curve.

To investigate the changes in the crystal structure and the hydrogen content, in situ XRD measurements were conducted under a $H_2$ atmosphere in the temperature range from room temperature to 300 °C under 0.1 MPa-$H_2$ using a multipurpose X-ray diffractometer (PANalytical, Empyrean). To obtain the fully hydride phase of the γ phase, the sample was heated to 300 °C under 0.1 MPa-$H_2$ and then cooled to room temperature. After this pretreatment, XRD patterns were acquired at temperatures ranging from the phase-transition temperatures determined from the DSC curve.

The hydrogen desorption properties were evaluated by $H_2$ temperature-programmed desorption ($H_2$-TPD). To obtain the fully hydride phase of the γ phase, the powder sample was heated at 300 °C for 1 h under a $H_2$ flow at 0.1 MPa and 30 mL/min. The sample was then cooled to room temperature under the same flow. The gas flow was switched from $H_2$ to Ar at room temperature, and the change of the crystal structure was determined by powder XRD measurement. Following this measurement, the sample was heated at 5 °C/min under an Ar flow at 0.1 MPa and 30 mL/min. The hydrogen desorbed from a metal lattice was monitored by in-line gas chromatography (Shimadzu GC-8A, thermal conductivity detector, Shincarbon-ST column, Ar carrier gas). The hydrogen content of the sample at each temperature was calculated from the TPD spectrum as a function of temperature by

$$\text{Hydrogen content(T)}\quad [\mathrm{H}/\mathrm{M}] = H_0\left(1-\int_{25\,^\circ\mathrm{C}}^{T\,^\circ\mathrm{C}} Intensity(T)\mathrm{d}T \Big/ \int_{25\,^\circ\mathrm{C}}^{420\,^\circ\mathrm{C}} Intensity(T)dT\right) \quad (1)$$

where $H_0$ is the initial hydrogen content at 25 °C under an Ar flow.

### 2.3. Catalytic properties

The catalytic properties of $Zr_7Ni_{10}$ in the hydrogenation of acetylene were evaluated using a fixed-bed flow reactor. Pulsed gas tests were conducted to investigate the effect of absorbed hydrogen on the catalytic properties. As pretreatment, 0.25 g of the sample was heated at 300 °C for 1 h under a $H_2$ flow at 0.1 MPa and 30 mL/min. The degassed alloy phase, which desorbs hydrogen from the bulk, was prepared by the following method: The $H_2$ flow was switched to an Ar flow at 300 °C, and the sample was heated for an additional 1 h to release absorbed hydrogen completely (confirmed by XRD measurements). The sample

was then cooled in the furnace to room temperature. The α phase was prepared by cooling under the $H_2$ flow and then switching the $H_2$ to Ar at room temperature (details are explained in Fig. 5). To compare the catalytic activities of the degassed alloy phase and the α phase, they were heated under an Ar flow and 1.34 mL quantities of the pulsed reaction gas (2.0 % $C_2H_2$ / 80 % $H_2$ / 18 % Ar) were introduced into the Ar flow at temperatures up to 300 °C. The catalytic properties of the degassed alloy phase at each temperature were evaluated after the sample was heated to 300 °C to desorb hydrogen, whereas those of the α phase were evaluated during the heating and cooling process. The products were analyzed by in-line gas chromatography. The conversion of $C_2H_2$ and the selectivity of $C_2H_4$ and $C_2H_6$ were defined as

$$C_2H_2 \text{ Conversion } [\%] = ([C_2H_2 \text{ (feed)}]_{mol} - [C_2H_2]_{mol})/[C_2H_2 \text{ (feed)}]_{mol} \times 100 \quad (2)$$

$$C_2H_4 \text{ Selectivity } [\%] = [C_2H_4]_{mol}/([C_2H_4]_{mol} + [C_2H_6]_{mol}) \times 100 \quad (3)$$

$$C_2H_6 \text{ Selectivity } [\%] = [C_2H_6]_{mol}/([C_2H_4]_{mol} + [C_2H_6]_{mol}) \times 100 \quad (4)$$

The carbon loss $C_{loss}$ was estimated by

$$C_{loss} [\%] = ([C_2H_2 \text{ (feed)}]_{mol} - [C_2H_4]_{mol} - [C_2H_6]_{mol})/[C_2H_2 \text{ (feed)}]_{mol} \times 100 \quad (5)$$

The constant flow test was performed to examine the catalytic properties under the conditions where the hydrogen content varied. The fully hydride phase of the γ phase was prepared by heating the sample to 300 °C at 0.1 MPa-$H_2$ for 1 h and then cooling it to room temperature. The reaction gas (2.0 % $C_2H_2$ / 80 % $H_2$ / 18 % Ar) was introduced at a total pressure of 0.1 MPa and a total flow rate of 30 mL/min. The products were analyzed in the temperature range from room temperature to 300 °C during two cycles of the heating and cooling process. The surface morphological characterization of the $Zr_7Ni_{10}$ alloy under different states was carried out using scanning electron microscopy (SU-6600, Hitachi). The change in surface area was investigated by the Brunauer–Emmett–Teller method (BET method; BELSORP-max).

## 3. Results and discussion

### 3.1. Hydrogen storage properties

Fig. 1(a) shows XRD patterns for $Zr_7Ni_{10}$ after annealing and after the pretreatment for preparing the γ phase. The XRD pattern after annealing is consistent with the pattern reported previously, and no impurity peaks are observed, indicating a single phase of $Zr_7Ni_{10}$ [21]. The lattice parameters for the obtained sample were calculated to be $a = 12.37$ Å, $b = 9.176$ Å, $c = 9.204$ Å, and $V = 1044.4$ Å$^3$ ($R_p = 2.652$), which are similar to the parameters reported in a previous study [21]. The XRD pattern after pretreatment differed substantially from the pattern for the sample after annealing. This different pattern originates from the γ phase, as revealed in subsequent experiments (Fig. 3 and Fig. 4). Thus, at the beginning of each test, after the pretreatment was applied, the samples were expected to be the γ phase.

Fig. 2 presents the results of the PCI measurements for the $Zr_7Ni_{10}$–$H_2$ system at 150, 200, and 300 °C. The PCI at 150 °C during the absorption process showed a plateau from the α phase to the γ phase, whereas the PCI during the desorption process showed two plateaus associated with the β phase in 0.6–0.7H/M. In addition, the solid-solution region in the absorption process was broad, ranging to 0.56H/M at 0.8 MPa-$H_2$; the corresponding region in the desorption process was from 0.4H/M at 0.04 MPa-$H_2$. These features are consistent with the PCIs in previous reports [20]. The PCIs acquired at 200 °C and 300 °C showed the solid-solution region in the measurement pressure range and showed no hysteresis between the absorption and desorption processes. Compared with the PCIs at the same hydrogen pressure used in the constant flow test (approximately 0.1 MPa-$H_2$), the hydrogen content changed depending on temperature. At 150 °C, in particular, the hydrogen content differed substantially: 0.42H/M in the absorption process by the α phase and 0.63H/M in the desorption process by the β phase. Therefore, under the condition of the constant flow test, the hydrogen content of $Zr_7Ni_{10}$ varies with the phase transitions associated with the β phase and the broad solid-solution region of the α phase.

Fig. 3 shows the DSC curve under 0.1 MPa-$H_2$. Positive peaks represent exothermic reactions, which correspond to phase transitions with hydrogen absorption, and negative peaks represent endothermic reactions, which correspond to phase transitions with hydrogen desorption. In the heating process, peaks corresponding to phase transitions with hydrogen desorption from the γ phase to the β phase and that from the β phase to the α phase were observed at approximately 129 °C and 184 °C, respectively. By contrast, in the cooling process, a peak corresponding to a phase transition with hydrogen absorption from the α phase to the γ phase was observed at approximately 74 °C. This phase-transition process is consistent with the PCI acquired at 150 °C (Fig. 2). In addition, each phase-transition temperature for the sample during the catalytic reaction (described later in Fig. 9) was identified, along with the corresponding changes in hydrogen content across these temperatures.

Fig. 4 shows the results of in situ XRD measurements under 0.1 MPa-$H_2$ during the heating process and the cooling process after the pretreatment. The XRD pattern obtained at 25 °C differed substantially from that for the alloy phase (Fig. 1). The XRD pattern acquired at 150 °C during the heating process changed from that obtained at 25 °C and differed from that for the alloy phase. Thus, on the basis of the phase-transition process for the $Zr_7Ni_{10}$–$H_2$ system and the phase-transition

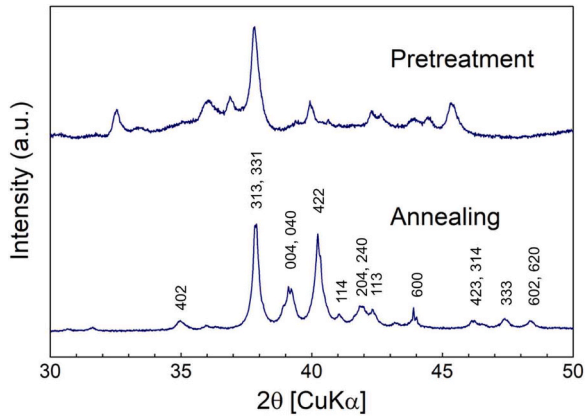


**Fig. 1.** XRD patterns for $Zr_7Ni_{10}$ before and after the pretreatment for preparing the γ phase. These measurements for both samples were conducted at room temperature under 0.1 MPa-$H_2$.

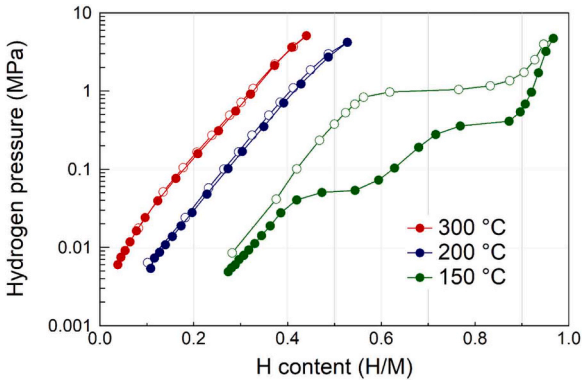


**Fig. 2.** PCI data for the $Zr_7Ni_{10}$–$H_2$ system at 150 °C, 200 °C, and 300 °C. The open circles indicate the measurement points during the absorption process, and the filled circles indicate those during the desorption process.

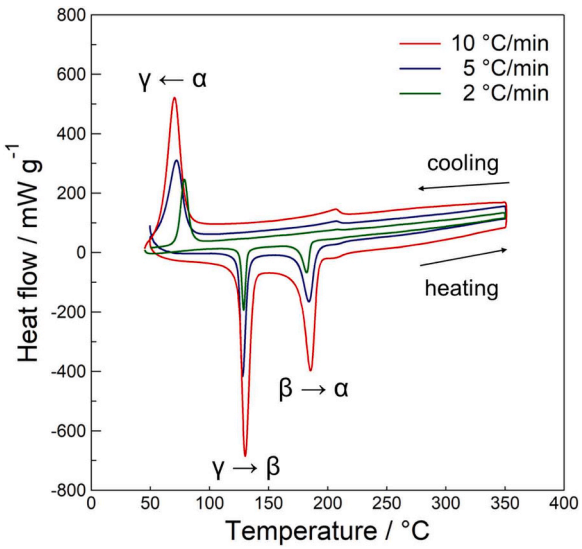


**Fig. 3.** DSC curves for the $Zr_7Ni_{10}$–$H_2$ system under 0.1 MPa-$H_2$. The positive peaks correspond to the phase transition with absorption of hydrogen, and the negative peaks correspond to the phase transition with desorption of hydrogen.

temperature obtained from the DSC curve (Fig. 3) during the dehydrogenation process, the XRD patterns acquired at 25 °C and 150 °C originated from the γ phase and the β phase, respectively. (Although the crystal structures of both phases are still unclear and structural analysis is essential for a comprehensive understanding of this alloy, it is beyond the scope of the present study.) The XRD patterns acquired at temperatures higher than 200 °C during the heating process changed again, and these peaks were basically indexed to the α phase. In addition, peak shifts to higher angles were observed as the temperature was increased, indicating a contraction of the lattice volume for the α phase. This behavior is consistent with the PCIs corresponding to 200 °C and 300 °C (Fig. 2), which show that the hydrogen content decreased from 0.27H/M to 0.18H/M. However, a detailed examination of the XRD patterns for the alloy phase (Fig. 1) reveals that the (114) peak was not observed in the pattern acquired at temperatures higher than 200 °C (Fig. 4(a)), suggesting that the change in the crystal structure of the α phase occurred during phase transitions. The crystal structure of the α phase after phase transitions to the hydride phases has been reported to be tetragonal, derived from a half-cell of the alloy phase's orthorhombic structure [21]. During the cooling process, the α phase existed from 300 °C to 150 °C and the peaks shifted to lower angles with decreasing temperature. This behavior indicates that the hydrogen content of the α phase increased. The β phase was not observed at any temperature during the cooling process. On the basis of the phase-transition behavior observed in the DSC curve (Fig. 3), the α phase is considered to have directly transformed to the γ phase during the cooling to 25 °C. This phase-transition behavior of the $Zr_7Ni_{10}$–$H_2$ system observed in the XRD measurements is also consistent with that observed in the PCIs (Fig. 2).

Fig. 5 shows the variation in the lattice parameters and unit cell volume of the α phase with different hydrogen contents. (The lattice parameters of the β and γ phases are not shown because their crystal structures have not yet been determined.) The lattice parameters and unit cell volume of the α phase exhibit a linear relationship with hydrogen content. The lattice parameters increase by approximately 0.05 Å per 0.1H/M along each axis, indicating that hydrogen absorption leads to an isotropic expansion of the α phase. The volume expansion of the unit cell per 0.1H/M is per hydrogen atom is approximately 2.4 $Å^3$, which is a reasonable value for the volumetric expansion caused by hydrogen absorption in metals [31,32].

The PCIs and the in situ XRD results reveal that the $Zr_7Ni_{10}$–$H_2$ system exhibits the unique feature of a continuously fluctuating hydrogen content. We therefore examined the hydrogen release performance for the $Zr_7Ni_{10}$–$H_2$ system. Fig. 5 shows the change in the XRD pattern for the sample after the hydrogenation and exposure to Ar at

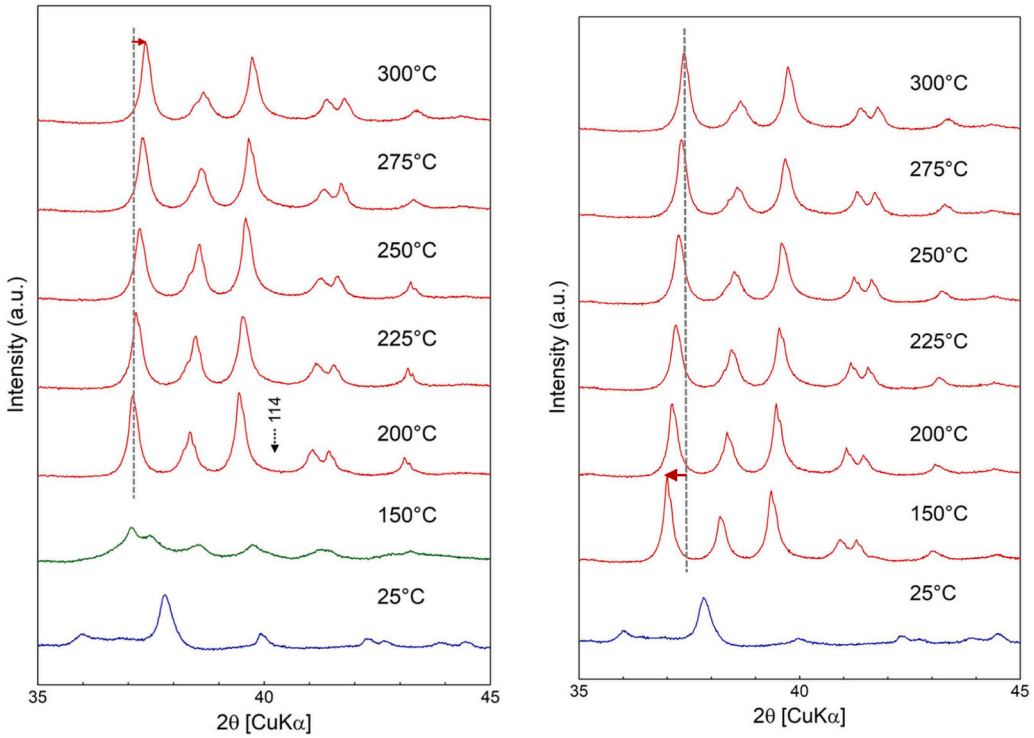


**Fig. 4.** XRD patterns for $Zr_7Ni_{10}$ under 0.1 MPa-$H_2$ during (a) the heating process and (b) the cooling process. The red, green, and blue lines correspond to the XRD patterns for the α phase, the β phase, and the γ phase, respectively.

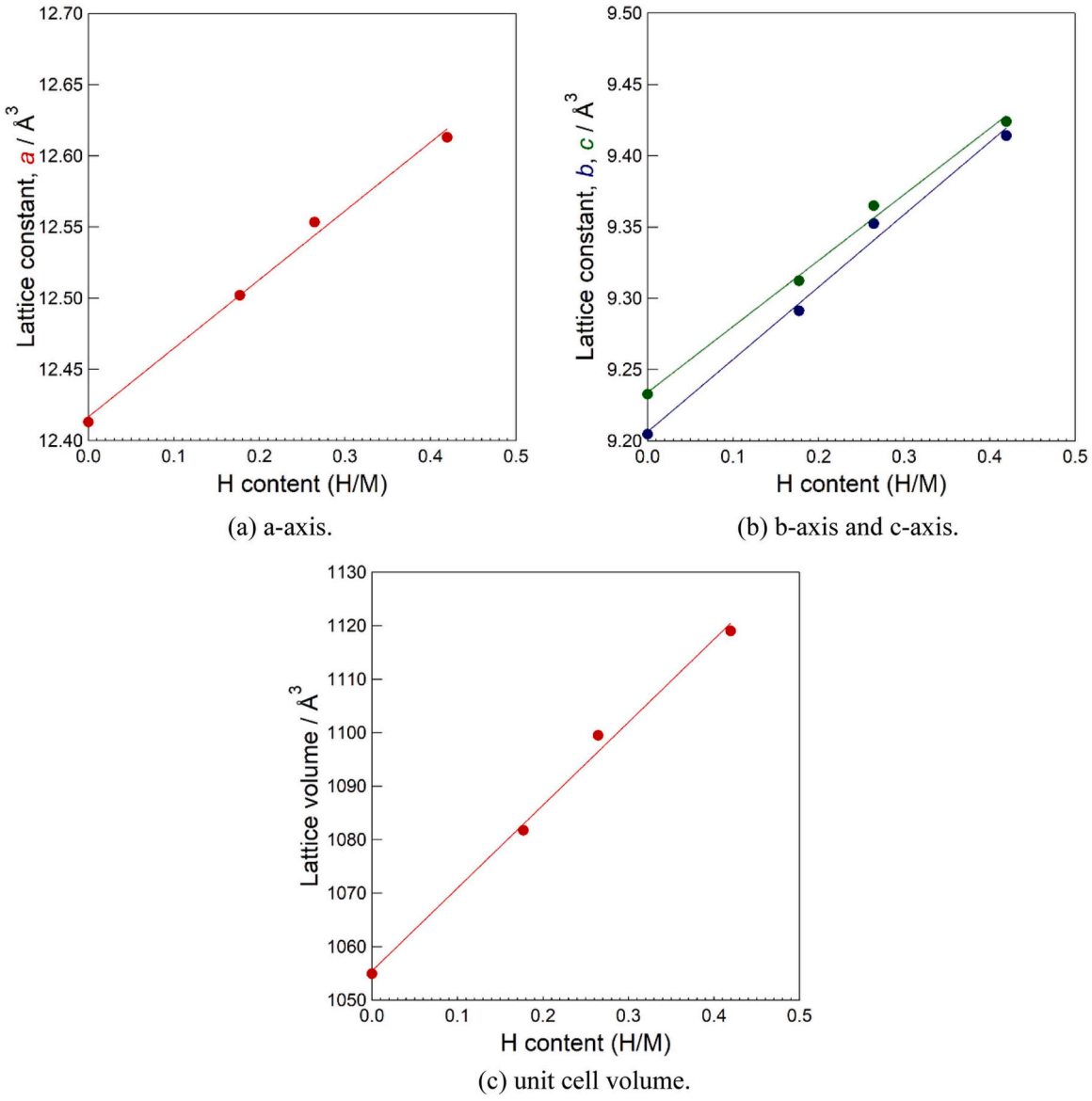


**Fig. 5.** Variation in lattice parameters and unit cell volume of the α phase: (c) a-axis, (d) b-axis and c-axis, (e) unit cell volume. Lattice parameters are determined by Rietveld analysis, and the hydrogen content was determined by the PCIs shown in Fig. 2.

room temperature. A comparison of these results with the $H_2$-XRD results in Fig. 4 indicates that both the β phase and the γ phase disappeared and that the α phase appeared. These results suggest that two hydride phases are not stable under an Ar atmosphere and require $H_2$ in the gas phase, even at room temperature. However, the peak positions are located at lower angles compared with those in the XRD pattern for the alloy phase (Fig. 1), indicating that hydrogen remained in the lattice and that the patterns originated from the α phase. The lattice parameters of the α phase after exposure to Ar at room temperature were a = 12.64 Å, b = 9.481 Å, c = 9.509 Å, and V = 1139.6 Å$^3$. Based on the lattice expansion of approximately 2.4 Å$^3$ per a hydrogen atom (Fig. 5), the hydrogen content in the α phase was estimated to be approximately 0.5H/M, which is nearly identical to the solubility limit of hydrogen in the α phase. We subsequently investigated the hydrogen desorption behavior of the α phase under an Ar atmosphere.

Fig. 6 shows the results of $H_2$-TPD experiments for the α phase. The peaks indicate the temperatures at which hydrogen in the lattice is released into the gas phase, and the peak intensity corresponds to the amount of released hydrogen. The α phase started to release hydrogen at approximately 50 °C and continued until the temperature reached

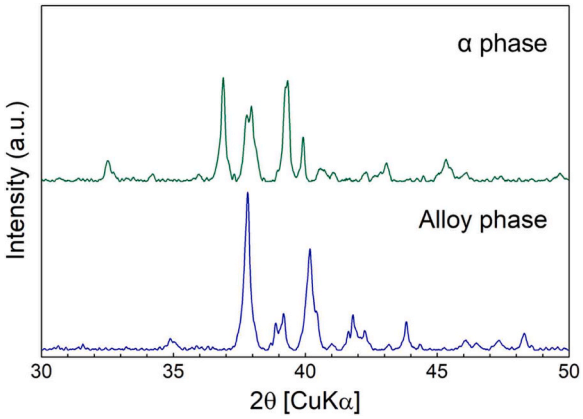


**Fig. 6.** Change in the XRD pattern for $Zr_7Ni_{10}$ after hydrogenation and exposure to Ar at room temperature, indicating dehydrogenation to the α phase.

approximately 350 °C. Given that the TPD spectrum was smooth, the release of absorbed hydrogen occurred continuously. The hydrogen content was estimated on the basis of the integrated area of the TPD spectrum. The initial hydrogen content ($H_0$) was assumed to be 0.5H/M, as determined by the XRD pattern (Fig. 6). Fig. 7 shows that the hydrogen content decreased to approximately 0.2H/M at 200 °C (the pulsed gas test condition described in Fig. 8), and most of the hydrogen was desorbed by approximately 350 °C.

### 3.2. Catalytic properties

The DSC (Fig. 3) and in situ XRD (Fig. 4) experiments showed that $Zr_7Ni_{10}$ undergoes complex phase transitions among three phases (i.e., α, β, and γ phase) and the hydrogen content of the α phase widely fluctuates depending on temperature. We subsequently investigated the effect of these properties on the catalytic behavior of the $Zr_7Ni_{10}$ alloy by using it as a catalyst in the hydrogenation of acetylene.

To examine the effect of the presence of absorbed hydrogen on the catalytic activity of $Zr_7Ni_{10}$, we conducted pulsed gas tests. Fig. 8 shows the results of pulsed gas tests for the degassed alloy phase and the α phase, which were prepared by controlling the atmosphere (refer to Section 2.3). As shown in Fig. 8(a), the α phase demonstrated approximately fivefold higher acetylene conversion than the degassed alloy phase at 200 °C. Although the hydrogen content of the α phase was difficult to determine exactly, the TPD spectrum indicated that the α phase retained hydrogen corresponding to approximately 0.2H/M at 200 °C (Fig. 7). The results of the pulsed gas tests suggest that absorbed hydrogen significantly enhances the catalytic activity of $Zr_7Ni_{10}$. However, with increasing temperature from 200 °C, the conversion decreased and it was lower during the cooling process than during the heating process. On the basis of the comparison of the catalytic activity between the degassed alloy phase and the α phase, the decrease in the catalytic activity of the α phase is speculatively attributed to the decrease in its hydrogen content. The $H_2$-TPD spectrum (Fig. 7) indicates that the α phase continues to desorb hydrogen up to approximately 350 °C. Thus, the pulsed gas tests suggest that the hydrogen content may play an important role in the catalytic properties. However, as shown in Fig. 8(b), the selectivity of ethylene and ethane did not differ between the degassed alloy phase and the α phase. Although the temperature dependence of the selectivity could not be evaluated because the limited amounts of products precluded an accurate analysis using the pulsed gas, the results suggest that absorbed hydrogen does not affect selectivity in the hydrogenation of acetylene.

The results of the pulsed gas tests (Fig. 8) indicate that absorbed hydrogen in $Zr_7Ni_{10}$ enhanced the reactivity of acetylene. We subsequently conducted a constant flow test to examine the effect of the unique hydrogen storage properties of the $Zr_7Ni_{10}$ alloy on its catalytic properties. Fig. 9 shows the results of a constant flow test for the sample after the pretreatment. The conversion of acetylene (Fig. 9(a)) increased with increasing temperature and reached 93 % at 230 °C. However, at temperatures greater than 230 °C, the conversion of acetylene decreased. Interestingly, the conversion of acetylene during the cooling process was nearly identical to that during the heating process. The same feature appeared in the second cycle, indicating the catalytic activity behavior is reversible. Fig. 9(b) shows the selectivity in this reaction. Although the selectivity of ethylene was slightly improved at higher temperatures, no substantial difference was observed in factors such as the conversion of acetylene. The selectivity in the second cycle was nearly identical to that observed in the first cycle. As also indicated by the pulsed gas tests (Fig. 8), absorbed hydrogen in this alloy is considered not to affect the selectivity in the hydrogenation of acetylene.

On the basis of the hydrogen storage properties and catalytic properties of $Zr_7Ni_{10}$, the change in catalytic activity at temperatures higher than 230 °C is attributed to the change in the hydrogen content of the α phase. In general, such a decrease in catalytic activity is due to catalyst deactivation (e.g., carbon deposition or the production of green oil) [35, 36]. However, as shown in Fig. 9(a), the conversion of acetylene recovered during the cooling process. Thus, the increase in catalytic activity during the cooling process shown in Fig. 9(a) cannot be described by simple catalyst deactivation. Such behavior has already been reported and was concluded to be caused by the temperature dependence of the average surface coverage of reactive species [37,38]. With increasing temperature, the average surface coverage (defined as the product of the incident flux and the residence time) decreased, resulting in a lower reaction rate. However, on the basis of the pulsed gas tests (Fig. 7), compared with the average surface coverage, the variation in the hydrogen content of $Zr_7Ni_{10}$ is considered to more strongly influence the catalytic activity in this temperature range. As shown in Fig. 8(a), the catalytic activity of the degassed alloy phase is approximately the same during the heating process from 200 °C to 300 °C, indicating that the average surface coverage of acetylene does not change in this hydrogenation reaction. Instead, as revealed in the pulsed gas test for the α phase, the small amount of absorbed hydrogen enhances the catalytic activity and the hydrogen content plays a more dominant role. This trend is considered to be the same as that observed in the constant flow test (Fig. 9). In the temperature range above 230 °C, $Zr_7Ni_{10}$ existed as the α phase responsible for the peaks in the DSC profile (Fig. 3).In addition, the hydrogen content of the α phase decreased with increasing temperature and vice versa, as revealed by in situ XRD measurements (Fig. 4). Given these results, the variation of the hydrogen content of the α phase was responsible for the reversible catalytic activity behavior shown in Fig. 9. However, at temperatures below 230 °C, the phase transition between the β phase and the γ phase did not affect the catalytic activity because insufficient thermal energy was available to overcome the activation energy. Although this study could not equivalently examine the effect of the hydrogen content over the entire range including the α, β, and γ phases, the variation in the hydrogen content of the α phase is considered to induce the reversible catalytic activity behavior.

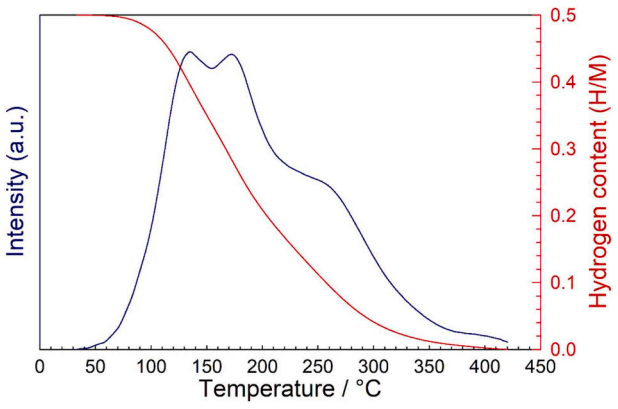


**Fig. 7.** $H_2$-TPD spectrum and change in hydrogen content of the α phase under an Ar flow. To estimate the change in hydrogen content, the initial hydrogen content ($H_0$) was assumed to be 0.5H/M from the the linear relationship between the hydrogen content and unit cell volume (Fig. 5).

## 4. Conclusion

This study focused on the $Zr_7Ni_{10}$ alloy, which undergoes unique phase-transition processes among the α, β, and γ phases and a broad solid-solution region, to investigate the effect of the variation in the hydrogen content on the alloy's catalytic performance. The absorbed hydrogen in $Zr_7Ni_{10}$ increased the conversion of acetylene, whereas the desorption of hydrogen decreased the conversion, indicating that the hydrogen content is a dominant factor affecting the catalytic activity in the hydrogenation of acetylene. Under a constant flow of reaction gas containing hydrogen, $Zr_7Ni_{10}$ showed a reversible catalytic activity behavior depending on temperature. Above 230 °C, where $Zr_7Ni_{10}$

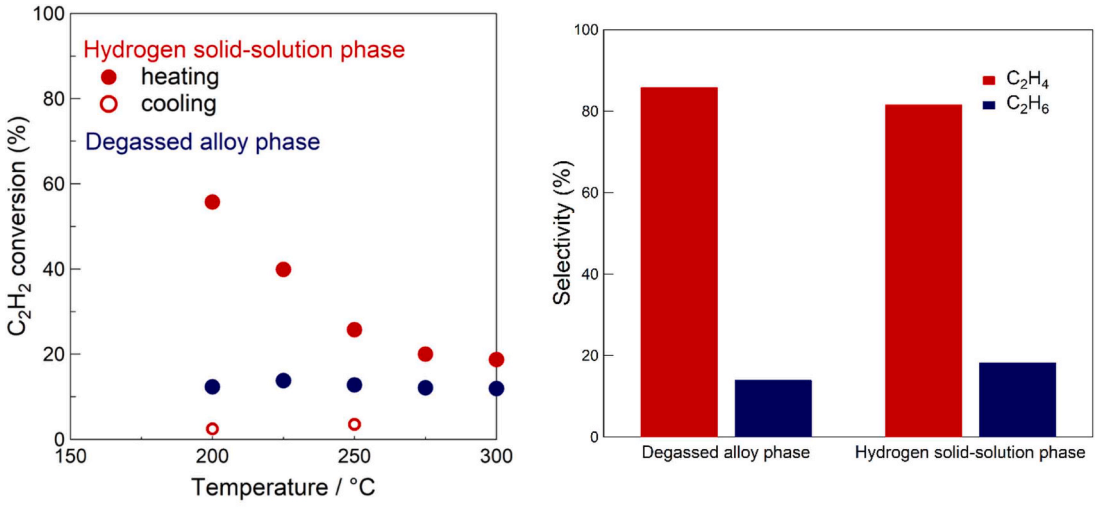


(a) Conversion of $C_2H_2$ pulsed gas (b) Selectivity of $C_2H_4$ and $C_2H_6$ at 200 °C

**Fig. 8.** Catalytic properties of the degassed alloy phase and the α phase in the hydrogenation of $C_2H_2$ pulsed gas: (a) conversion of $C_2H_2$ pulsed gas and (b) selectivity of $C_2H_4$ and $C_2H_6$ at 200 °C for the degassed alloy phase and the α phase during the heating process. $C_{loss}$ was 20–30 %, which was caused by oil production [33,34].

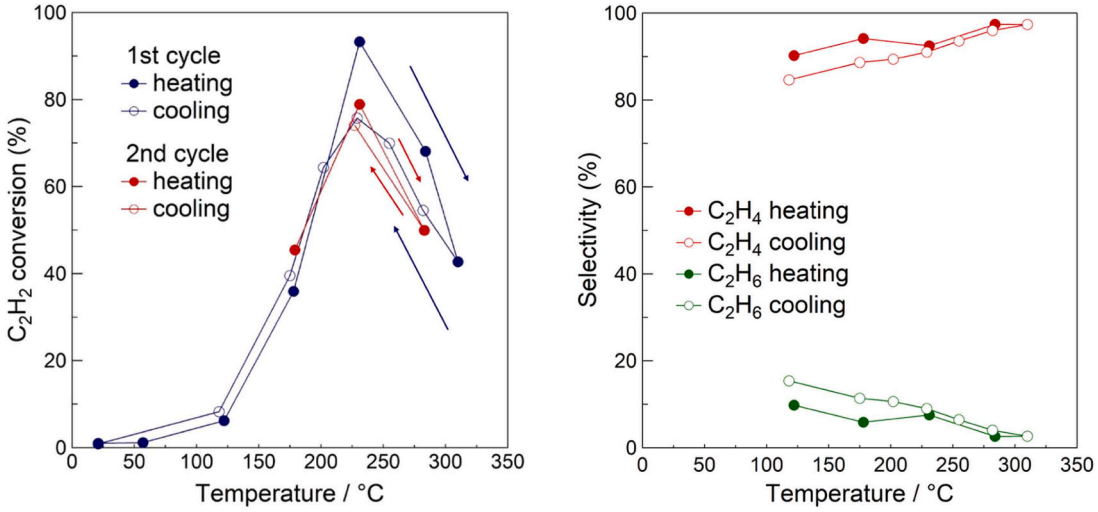


(a) $C_2H_2$ conversion. (b) Selectivity in the first cycle.

**Fig. 9.** Catalytic properties of $Zr_7Ni_{10}$. The mass and surface area of the sample were 0.25 g and 2.0 × $10^{-2}$ $m^2$, respectively. The composition of the reaction gas was 2.0 % $C_2H_2$ / 80 % $H_2$ / 18 % Ar at 30 mL/min and 0.1 MPa. $C_{loss}$ was 15–30 %, which was caused by oil production [33,34]. The selectivity in the second cycle was nearly identical to that observed in the first cycle.

existed as the α phase, the conversion of acetylene decreased with increasing temperature. During the cooling process, the conversion of acetylene recovered and was almost identical to that observed during the heating process. Given that the hydrogen content of the α phase substantially fluctuates with temperature and that a small amount of absorbed hydrogen enhances the catalytic activity, the variation in the hydrogen content of the α phase above 230 °C is considered to induce the reversible catalytic activity behavior.

## Declaration of Competing Interest

The authors declare that they have no known competing financial interests or personal relationships that could have appeared to influence the work reported in this paper.

## Acknowledgement

The authors thanks Dr. Haruka Yoshikawa at Tokyo University of Science and Ms. Satoko Murata, Ms. Kanon Amai at IMRAM Tohoku University for helpful discussions and technical supports to perform this study. We are also grateful to Dr. Akira Yasui, Dr. Yasumasa Takagi, and Dr. Jiayi Tang of JASRI for helpful discussions and assistance during the HAXPES analyses performed on the 09XU beamline at the SPring-8 facility (proposal nos. 2021B1001, 2022B1045, 2023A1037, 2023B1042, 2023B1935, 2024A1669, and 2024B1581). This work was supported in part by Grants-in-Aid for Scientific Research (B) (nos. 22H01804 and 22H04581) from the Ministry of Education, Culture, Sports, Science and Technology (MEXT) of Japan and from JST CREST (no. JPMJCR22O3), by the Dynamic Alliance for Open Innovation Bridging Human, Environment and Materials.

## Appendix A. Supporting information

Supplementary data associated with this article can be found in the online version at doi:10.1016/j.nxmate.2025.101313.

## References


[1] V.T. Coon, T. Takeshita, W.E. Wallace, R.S. Craig, J. Phys. Chem. 80 (1976) 1878–1879, https://doi.org/10.1021/j100558a013.
[2] I.R. Konenko, N.M. Parfenova, E.I. Klabunovskii, E.M. Savitskii, V.F. Terekhova, I. A. Markova, V.P. Mordovin, D.E. Bogatin, Bull. Acad. Sci. USSR Div. Chem. Sci. 27 (1978) 1473–1474, https://doi.org/10.1007/BF00946910.
[3] K. Soga, K. Otsuka, M. Sato, T. Sano, S. Ikeda, J. Less Common Met. 71 (1980) 259–263, https://doi.org/10.1016/0022-5088(80)90209-X.
[4] C.-M. Chen, J.-M. Jehng, Appl. Catal. A Gen. 267 (2004) 103–110, https://doi.org/10.1016/j.apcata.2004.02.038.
[5] N. Endo, S. Ito, S. Kameoka, A.P. Tsai, T. Hirata, C. Nishimura, Catal. Today 164 (2011) 293–296, https://doi.org/10.1016/j.cattod.2010.11.039.
[6] N. Endo, S. Kameoka, A.P. Tsai, T. Hirata, C. Nishimura, Mater. Trans. 52 (2011) 1794–1798, https://doi.org/10.2320/matertrans.MAW201105.
[7] R. Yamagishi, T. Kojima, S. Kameoka, D. Okuyama, T.J. Sato, C. Nishimura, A.-P. Tsai, Int. J. Hydrog. Energy 42 (2017) 21832–21840, https://doi.org/10.1016/j.ijhydene.2017.07.072.
[8] R. Tsukuda, T. Kojima, D. Okuyama, S. Kameoka, C. Nishimura, Int. J. Hydrog. Energy 45 (2020) 19226–19236, https://doi.org/10.1016/j.ijhydene.2020.05.062.
[9] E.D. Snijder, W.P.M.V. Swaaij, Chem. Eng. Sci. 48 (1993) 2429–2441, https://doi.org/10.1016/0009-2509(93)81064-3.
[10] R.M. Frak, J. Less Common Met. 109 (1985) 279–286, https://doi.org/10.1016/0022-5088(85)90060-8.
[11] K. Soga, H. Imamura, S. Ikeda, J. Phys. Chem. 81 (1977) 1762–1766, https://doi.org/10.1021/j100533a010.
[12] S. Kato, S.K. Matam, P. Kerger, L. Bernard, C. Battaglia, D. Vogel, M. Rohwerder, A. Züttel, Angew. Chem. Int. Ed. 55 (2016) 6028–6032, https://doi.org/10.1002/anie.201601402.
[13] S. Kato, A. Borgschulte, D. Ferri, M. Bielmann, J.-C. Crivello, D. Wiedenmann, M. Parlinska-Wojtan, P. Rossbach, Y. Lu, A. Remhof, A. Züttel, Phys. Chem. Chem. Phys. 14 (2012) 5518–5526, https://doi.org/10.1039/c2cp23264b.
[14] R. Tsukuda, T. Kojima, Y. Xu, C. Nishimura, M. Krajcí, S. Kameoka, J. Phys. Chem. C. 125 (2021) 20919–20929, https://doi.org/10.1021/acs.jpcc.1c06484.
[15] H.A. Aleksandrov, S.M. Kozlov, S. Schauermann, G.N. Vayssilov, K.M. Neyman, Angew. Chem. Int. Ed. 53 (2014) 13371–13375, https://doi.org/10.1002/anie.201405738.
[16] G. Qing, C. Ruting, G. Jianping, Q. Chao, X. Zhitao, Y. Hanxue, G. Wenbo, P. Qijun, W. Anan, C. Ping, J. Am. Chem. Soc. 143 (2021) 20891–20897, https://doi.org/10.1021/jacs.1c09489.
[17] Y. Hongen, L. Xingguo, Z. Jie, ACS Catal. 14 (2024) 3139–3157, https://doi.org/10.1021/acscatal.3c05696.
[18] F.H.M. Spit, J.W. Drijver, S. Radelaar, Scr. Metall. 14 (1980) 1071–1076, https://doi.org/10.1016/0036-9748(80)90208-2.
[19] J.M. Joubert, M. Latroche, A. Percheron-Guégan, J. Alloy. Compd. 231 (1995) 494–497, https://doi.org/10.1016/0925-8388(95)01866-2.
[20] H.T. Takeshita, T. Kiyobayashi, H. Tanaka, N. Kuriyama, M. Haruta, J. Alloy. Compd. 311 (2000) L1–L4, https://doi.org/10.1016/S0925-8388(00)01083-5.
[21] H.T. Takeshita, N. Fujiwara, T. Oishi, D. Noréus, N. Takeichi, N. Kuriyama, J. Alloy. Compd. 360 (2003) 250–255, https://doi.org/10.1016/S0925-8388(03)00358-X.
[22] H.T. Takeshita, N. Fujiwara, N. Takeichi, H. Senoh, T. Oishi, J. Alloy. Compd. 404-406 (2006) 609–612, https://doi.org/10.1016/j.jallcom.2005.02.080.
[23] K. Young, T. Ouchi, Y. Liu, B. Reichman, W. Mays, M.A. Fetcenko, J. Alloy. Compd. 480 (2009) 521–528, https://doi.org/10.1016/j.jallcom.2009.01.117.
[24] J. Nei, K. Young, R. Regmi, G. Lawes, S.O. Salley, K.Y.S. Ng, Int. J. Hydrog. Energy 37 (2012) 1042–16055, https://doi.org/10.1016/j.ijhydene.2012.08.024.
[25] A. Altomare, C. Cuocci, C. Giacovazzo, A. Moliterni, R. Rizzi, N. Corriero, A. Falcicchio, J. Appl. Crystallogr. 42 (2013) 1231–1235, https://doi.org/10.1107/S0021889813013113.
[26] M.E. Kirkpatrick, J.F. Smith, W.L. Larsen, Acta Crystallogr. 15 (1962) 894–903, https://doi.org/10.1107/S0365110X62002339.
[27] J.L. Glimois, P. Forey, J. Feron, C. Becle, J. Less Common Met. 78 (1981) 45–50, https://doi.org/10.1016/0022-5088(81)90112-0.
[28] J.-M. Joubert, R. Cerný, K. Yvon, M. Latroche, A. Percheron-Guégan, Acta Crystallogr. Sect. C. Cryst. Struct. Commun. 53 (1997) 1536–1538, https://doi.org/10.1107/S0108270197007142.
[29] P.M.D. Wolff, Y. Billiet, J.D.H. Donnay, W. Fischer, R.B. Galiulin, A.M. Glazer, M. Senechal, D.P. Shoemaker, H. Wondratschek, T. Hahn, A.J.C. Wilson, S. C. Abrahams, Acta Crystallogr. Sect. A Found. Crystallogr. 45 (1989) 494–499, https://doi.org/10.1107/S0108767389002230.
[30] P.M.D. Wolff, Y. Billiet, J.D.H. Donnay, W. Fischer, R.B. Galiulin, A.M. Glazer, T. Hahn, M. Senechal, D.P. Shoemaker, H. Wondratschek, A.J.C. Wilson, S. C. Abrahams, Acta Crystallogr. Sect. A Found. Crystallogr. 48 (1992) 727–732, https://doi.org/10.1107/S0108767392003428.
[31] R. Griessen, R. Feenstra, J. Phys. F Met. Phys. 15 (1985) 1013–1019, https://doi.org/10.1088/0305-4608/15/4/024.
[32] G.J. Thomas, W.D. Drotning, Metall. Trans. A 14 (1983) 1545–1548, https://doi.org/10.1007/BF02654380.
[33] A.J. McCue, J.A. Anderson, Front. Chem. Sci. Eng. 9 (2015) 142–153, https://doi.org/10.1007/s11705-015-1516-4.
[34] S. Hwang, Y.B. Hwang, H.W. Hwang, D. Kim, J.Y. Lee, J. Hwang, E.D. Park, S. K. Kim, Adv. Energy Sustain. 6 (2025) 2400341, 0.1002/aesr.202400341.
[35] A. Sárkány, A. Weiss, T. Szilágyi, P. Sándor, L. Guczi, Appl. Catal. 12 (1984) 373–379, https://doi.org/10.1016/S0166-9834(00)81674-7.
[36] H.-X. Su, Y. Jiao, J.-G. Shi, Z.-W. Yuan, D. Zhang, X.-P. Wang, J. Ren, D. Liu, J.-Z. Gui, H.-Y. Gao, X.-L. Xu, Pet. Sci. 21 (2024) 1405–1414, https://doi.org/10.1016/j.petsci.2023.10.012.
[37] K.M. Bratlie, L.D. Flores, G.A. Somorjai, Surf. Sci. 599 (2005) 93–106, https://doi.org/10.1016/j.susc.2005.09.051.
[38] I. Bychko, P. Strizhak, Fuller. Nanotub. Carbon Nanostruct. 26 (2018) 804–809, https://doi.org/10.1080/1536383X.2018.1502176.